Gap plasmon polariton structure for very efficient microscale-to-nanoscale interfacing

Pavel Ginzburg, David Arbel, and Meir Orenstein

Department of Electrical Engineering, Microphotonics Laboratory, Technion-Israel Institute of Technology, Haifa 3200, Israel

Received June 19, 2006; revised August 14, 2006; accepted August 26, 2006; posted August 30, 2006 (Doc. ID 72123); published October 26, 2006

The seamless transition between microscale photonics and nanoscale plasmonics requires overpassing different waveguiding mechanisms and a few orders of magnitude in the lateral dimension. Exploiting gap plasmon–polariton waves both at the microscale and nanoscale with an ultrashort (few micrometers) nonadiabatic tapered gap plasmon waveguide, we show theoretically that very high-power transfer efficiency (~70%) is achieved. The same mechanism may be used to harvest impinging light waves and direct them into a nanhole or slit to exhibit an anomalous transmission without the conventional periodic structures. The interplay of plasmonic and oscillating modes is analyzed. © 2006 Optical Society of America

OCIS codes: 130.3120, 130.2790, 240.6680.

Surface-plasmon polariton (SPP) optical waves on a metal–dielectric interface may be confined much below the optical wavelength,[1] offering a route to nanophotonics. Metal stripes tens of nanometers thick can potentially serve as low-loss SPP waveguides,[2–4] and research of subwavelength SPP optics shows promise for the realization of nanometer-size-photonic circuits for applications such as optical interconnects, signal processing, and nanosensing.[5]

A major concern of basic interest and for practical implementation of plasmonic circuits is efficient interfacing between conventional micrometer-size photonics to tens-of-nanometers-size plasmonics. A related issue is the efficient transmission of light via nanoholes and slits in metal layers,[6] where the micrometer-scale impinging beam is harvested employing a periodic structure and then transmitted through the nanohole.[7] Several schemes for coupling light to stripe plasmon waveguides are reported.[4,8,9] While a significant portion of research was focused on slab and stripe plasmon waveguides consisting of a metal core with a dielectric cladding (Refs. 2–5 and 8 and references therein), we studied the inverted structure of a dielectric core with a metal cladding,[10] called the plasmon gap waveguide (PGW).[11] The PGW provides tight optical confinement by the metallic cladding and should be better coupled to a dielectric waveguide because of the continuity of the waveguide core as well as to regular plasmon waveguides by proper plasmonic coupling schemes.

We investigate the interplay and coupling of modes in a tapered PGW structure. A very short taper exhibits surprisingly high-efficiency plasmon-assisted coupling from a micrometer-size silica–air-clad dielectric waveguide to a 50 nm silica–gold-clad PGW. A power transfer efficiency of ~70% is calculated. Some of the fundamental findings are a cutoff of an oscillatory mode, which is transformed into a plasmon surface wave; relaxation of adiabaticity constraints for efficient PGW tapers; and a novel highly efficient harvesting of light into nanoslits—without a periodic structure—namely, funnel-shaped metal interfaces that can be used to transmit more than 100% via nanoholes.

The dispersion relations of PGWs were discussed in different contexts.[12–14] The guided modes are either plasmon modes of exponential nature or oscillating modes with a trigonometric behavior. Recently, analysis of the trade-off between confinement and propagation losses in a PGW[15] and including the effects of empirical metal data was reported.[16] We emphasize an important difference between a metal slab and gap structures, namely, a global mode cannot be practically excited in a microscale metal slab owing to the fast decay of the field in a metal core thicker than the skin depth (~100 nm). Thus two independent single surface modes will propagate instead. In contrast, a gap structure robustly supports global plasmonic modes for both nanoscale and microscale waveguides [see Fig. 1(a)], an essential characteristic for the desired seamless dimension transition.

The PGW consists of a planar silica slab with a width of $2d$ along the X axis surrounded on both sides by a semi-infinite gold cladding with the waves propagating along the Z axis. At the wavelength of 1.55 μm, the dielectric constants are $\varepsilon_d(SiO_2)=2.085$

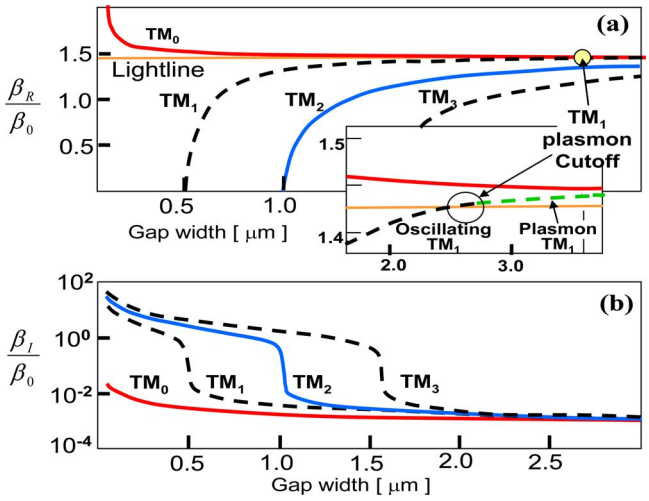

Fig. 1. (Color online) (a) Real and (b) imaginary part of propagation constants of various modes versus the width of PGW. The inset shows the cutoff region of the asymmetric plasmon mode.

0146-9592/06/223288-3/$15.00

and $\varepsilon_m(\text{gold}) = -132 - i12.6$.[17] The PGW also supports oscillating TE modes, but we will focus on TM modes (plasmon modes are TM) with $\vec{E} = \hat{x} f(x) e^{-i\beta z}$ and $\vec{H} = \hat{y} g(x) e^{-i\beta z}$, where $\beta = \beta_R - i\beta_I$ is the complex propagation constant.

The dispersion relations for the symmetric guided modes are[14]

$$\text{plasmon:} \quad tgh(k_p d) = -(k_m/\epsilon_m)/(k_p/\epsilon_d), \qquad (1a)$$

$$\text{oscillating:} \quad tg(k_O d) = -(k_m/\epsilon_m)/(k_O/\epsilon_d), \qquad (1b)$$

where $k_p^2 = \beta^2 - k_0^2\epsilon_d$; $k_O^2 = k_0^2\epsilon_d - \beta^2$; $k_m^2 = \beta^2 - k_0^2\epsilon_m$. β_R and β_R versus the gap width (which we intend to vary linearly) are plotted in Figs. 1(a) and 1(b), respectively. In Fig. 1(a), the plasmon and oscillating modes are seperated by the core light line with $\beta_{R,\text{plasmon}} > k_0 n_d$ and $0 < \beta_{R,\text{oscillating}} < k_0 n_d$.

Two plasmon modes exist: symmetric with no cutoff and antisymmetric with a cutoff for gap widths below $\sim\lambda_0/2n_d$, making the first the single mode of the structure in the nanoregime. Oscillating modes exist as well in the PGW; each has a cutoff width below which it becomes evanescent with very high losses, as seen in Fig. 1(b). An interesting feature found here is that the antisymmetric plasmon mode, TM_1, for a gap width below the cutoff value, transforms into the first odd oscillating mode. This oscillating mode exhibits two cutoff values: from below—into an evanescent mode—and from above—into a plasmon mode. All the other oscillating modes approach the light line asymptotically but do not cross it.

The first stage of harvesting the light from the microscale silica–air dielectric waveguide calls for an efficient conversion of the photonic mode to a plasmonic mode supported by the PGW [Fig. 2(a)]. Due to the symmetry of the structure and excitation, only even modes are relevant—the symmetrical plasmon mode TM_0 and the lowest-order even oscillating mode TM_2 [Figs. 2(c) and 2(d)].

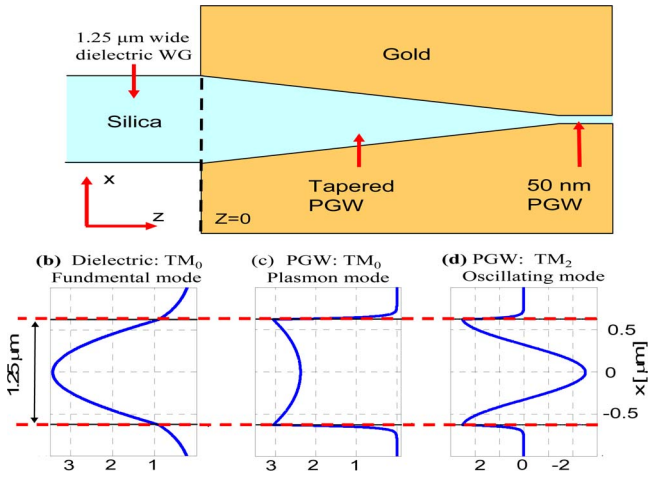

Fig. 2. (Color online) (a) Tapered plasmon gap waveguide, a 1.25 μm wide input dielectric waveguide, and a 50 nm output plasmon gap waveguide. (b)–(d) Magnetic field amplitude (H_y) profiles at PGW input plane: (b) symmetric dielectric, (c) symmetric plasmon, (d) symmetric oscillating.

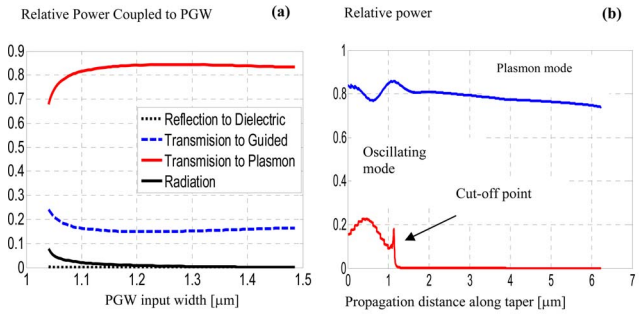

Fig. 3. (Color online) (a) PGW input optimization—dielectric input mode coupling to the plasmon and oscillating modes versus input width. (b) Intermode coupling and evolution versus taper propagation distance for the forward plasmon and oscillating modes.

We analyzed, in closed form using the transfer matrix formalism[18,19] (TMF), the transmission and reflection at the dielectric–plasmon waveguide interface. The incoming mode couples into both plasmon and oscillating modes of the PGW as well as being backreflected and coupled to guided and radiation modes of the dielectric slab. Figure 3(a) shows that at a waveguide width of 1.25 μm, almost no energy ($<1\%$) is backreflected in the photonic–plasmonic conversion, 84% of the incident power is converted to the plasmon mode of the PGW, and 15% is coupled to the oscillating mode.

The second stage of harvesting is the collection of the power converted to the plasmonic mode and guiding it with minimal losses into the 50 nm wide waveguide. A linearly tapered structure is employed. The Z-dependent width change also facilitates some coupling between the plasmon and oscillating modes in the PGW. We maintain this intermode coupling and optimize the taper angle to maximize plasmon mode transmission. The linearly tapered PGW was discretized to a sequence of short segments with varying width, and we employed a TMF to calculate the amplitudes of the forward and backward modes at each segment. Mode-coupling coefficients were calculated by overlap integrals of the form

$$C_{i,j}^{L,R} = \langle \epsilon_i^L | h_j^R \rangle = \int \int_{z=0} \epsilon_i^L \times h_j^R \mathrm{d}x, \qquad (2)$$

where ϵ_i^L is the electric field of mode i in the left segment, h_j^R is the magnetic field of mode j in the right segment, and i and j are modes. We did not assume orthogonality of the modes at each segment, and coupling coefficients within the segment $C_{i,j}^{L,L}$, $C_{i,j}^{R,R}$ were calculated and not assumed to be zero. This scheme fits lossy geometries well and also stabilizes the numerical procedure. Assuming mode orthogonality, the zero elements of the matrices accumulate numerical noise and grow over long propagation distances while for nonorthogonality these elements stay $\sim$12 orders of magnitude below the significant amplitudes.

The coupling of plasmon and oscillating modes along the tapered waveguide is exhibited by the power oscillation of the modes [Fig. 3(b)]. The optimal design obtained for a taper angle of 5.5° is a

trade-off between the maximal coupling and higher propagation losses of longer taper lengths. The cutoff point of the oscillating mode occurs approximately where the coupled power is maximal at the plasmonic mode [Fig. 3(b)]. This taper angle results in a very short 6 μm nonadiabatic funnel, an order of magnitude shorter than the common wisdom in regular photonics circuits. The two reasons for not requiring adiabaticity from plasmonic gap tapers are the dominance of the propagation loss and the absence of other forward propagation modes to couple to neither guided modes nor radiation. In a dielectric taper, the primary mechanism of nonadiabatic taper loss is the coupling to forward propagation radiation modes. More than 70% of the power incident from the dielectric waveguide is eventually coupled into the plasmon mode of the 50 nm wide PGW. To verify this result, finite-difference time-domain simulations of the tapered PGW coupler were performed, and confirmed the calculated results, exhibiting a coupling efficiency of ~70% [Fig. 4(a)]. Switching the input field from TM to TE results in an almost complete shutdown of the transmission with most power reflected back [Fig. 4(b)]. This validates that the high coupling efficiency is achieved by coupling to plasmon surface waves.

The high harvesting efficiency from a micrometer-scale input field into a 50 nm plasmon gap can also be used for anomalous transmission experiments via nanosized holes or slits in thin metal films.[7,8] In the latter, harvesting enhancement is achieved by a periodic array of grooves surrounding the slit coupling the impinging field into a surface plasmon polariton. The method described in our Letter of employing a funnel structure offers roughly an order-of-magnitude improvement over the theoretical calculations of periodic arrays while not being sensitive to wavelength. For input fields with lateral beam dimensions of ~1 μm, the periodic structure is almost inapplicable as the number of periods in the beam cross section is vanishingly small.

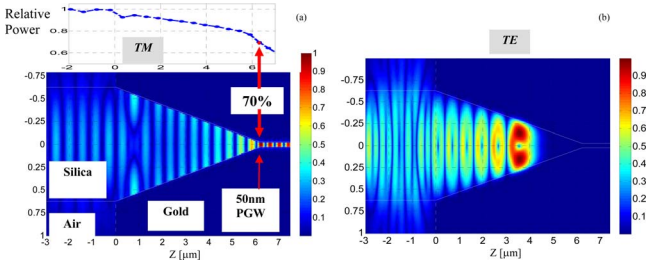

Fig. 4. (Color online) FDTD simulation result of the Poynting vector versus propagation along the tapered PGW coupler. (a) TM excitation with ~70% transmission. (b) TE excitation, no plasmon mode exists, oscillating mode is cut off and reflected.

Our analysis predicts a coupling loss of less than 2 dB from a micrometer-size dielectric waveguide to a 50 nm wide plasmon gap waveguide by a 6 μm short optimized tapered plasmon waveguide coupler. This is a promising method to couple micro-optics circuits to nano-plasmon-optics devices and a step toward large-scale integrated photonic circuits.

We thank the Israel Ministry of Science and the Eshcol scholarship program for partially supporting this research. D. Arbel's e-mail address is arbeld@tx.technion.ac.il.

References

1. H. Raether, *Surface Plasmons* (Springer-Verlag, 1988), Vol. 111.
2. J. J. Burke, G. I. Stegeman, and T. Tamir, Phys. Rev. B **33**, 5186 (1986).
3. P. Berini, Phys. Rev. B **61**, 10484 (2000).
4. R. Charbonneau, P. Berini, E. Berolo, and E. Lisicka-Skrzek, Opt. Lett. **25**, 844 (2000).
5. W. L. Barnes, A. Dereux, and T. W. Ebbesen, Nature **424**, 824 (2003).
6. T. W. Ebbesen, H. J. Lezec, H. F. Ghaemi, T. Thio, and P. A. Wolff, Nature **391**, 667 (1998).
7. F. J. Garcia-Vidal, H. J. Lezec, T. W. Ebbesen, and L. Martin-Moreno, Phys. Rev. Lett. **90**, 213901 (2003).
8. T. Nikolajsen, K. Leosson, I. Salakhutdinov, and S. I. Bozhevolnyi, Appl. Phys. Lett. **82**, 668 (2003).
9. M. Hochberg, T. Baehr-Jones, C. Walker, and A. Scherer, Opt. Express **12**, 5481 (2004).
10. P. Ginzburg, D. Arbel, and M. Orenstein, in *Integrated Photonics Research and Applications—IPRA 2005* (Optical Society of America, 2005), paper JWA6.
11. K. Tanaka and M. Tanaka, Appl. Phys. Lett. **82**, 1158 (2003).
12. E. N. Economou, Phys. Rev. **182**, 539 (1969).
13. I. P. Kaminow, W. L. Mammel, and H. P. Weber, Appl. Opt. **13**, 396 (1974).
14. B. Prade, J. Y. Vinet, and A. Mysyrowicz, Phys. Rev. B **44**, 13556 (1991).
15. R. Zia, M. D. Selker, P. B. Catrysse, and M. L. Brongersma, J. Opt. Soc. Am. A **21**, 2442 (2004).
16. J. A. Dionne, L. A. Sweatlock, H. A. Atwater, and A. Polman, Phys. Rev. B **73**, 035407 (2006).
17. E. D. Palik, *Handbook of Optical Constants of Solids* (Academic, 1985).
18. A. D. Oliver, *Microwave Horns and Feeds* (IEEE, 1994).
19. I. Breukelaar, R. Charbonneau, and P. Berini, Appl. Phys. Lett. **88**, 051119 (2006).